Piezoelectric Wireless Power Transfer using Halbach Array for the Internet of Implanted Things

Hailing Fu, *Member, IEEE,* George Gibson, Zhuowen Liu, Boli Chen, *Senior Member, IEEE,* Maobin Lu, Chen Chen, *Member, IEEE,* Dong Jiang, Nikolaos A. Chrysochoidis, Fang Deng, *Senior Member, IEEE*

Abstract—Implanted devices are increasingly used in chronic disease monitoring, but face challenges in energy autonomy. The paper presents a novel wireless power transfer method for self-sustained medical implants using Halbach array-based magnetic plucking and piezoelectric transduction. The wearable-implantable coupled system consists of a piezoelectric receiver within the implant to receive power and a near-field magnetic power transmitter as a wearable device. To deliver power over greater distances through the human body, the transmitter features a rotating magnetic Halbach array powered by a miniature motor or by human motion to generate an alternating magnetic field. The use of low-frequency rotating magnetic fields periodically excites a cantilevered piezoelectric beam with a tip magnet to realize wireless power transfer. A theoretical model that includes magnetic coupling, piezoelectric transduction and receiver beam dynamics has been established to study the electro-magneto-mechanical dynamics of this wireless power transfer system. The effectiveness of the Halbach array for extended power transfer is examined through theoretical modelling and numerical simulation, showing a 37.2% enhancement of the magnetic forces. A prototype was also fabricated and tested to examine the wireless power transfer performance. The established wireless power link can provide sufficient power ($\sim$32 μW) over a large transmission distance (22 mm), providing a potential battery-free solution for the self-sustained Internet of Implanted Things (IoIT) for personalized healthcare.

Index Terms—Wireless power transfer, implantable medical devices, Halbach array, piezoelectric transducers, self-sustained sensing, magnetic plucking, Internet of Implanted Things.

I. INTRODUCTION

IMPLANTABLE devices have been increasingly used inside human bodies to deal with chronic conditions, such as diabetes or coronary heart diseases [1]. These devices can form an Internet of Implanted Things (IoIT) to perform therapeutic

Hailing Fu, Zhuowen Liu, Maobin Lu, Chen Chen and Fang Deng are with the School of Automation, Beijing Institute of Technology, Beijing, 100081, China (e-mail: hailing.fu@bit.edu.cn).

George Gibson is with the Department of Electrical and Electronic Engineering, Imperial College London, SW7 2AZ, UK (e-mail: g.gibson23@ic.ac.uk).

Boli Chen is with the Department of Electronic and Electrical Engineering, University College London, WC1E 6BT London, U.K. (e-mail: boli.chen@ucl.ac.uk)

Dong Jiang is with the Institute of Sports Medicine, Beijing Key Laboratory of Sports Injuries, Peking University Third Hospital, Beijing, 100191 China (e-mail: bysyjiangdong@126.com).

Nikolaos A. Chrysochoidis is with Department of Mechanical Engineering and Aeronautics, University of Patras, Rion-Patras, Greece (e-mail: nchr@mech.upatras.gr).

functions or to monitor critical physiological parameters [2]. IoIT is a subset of the Internet of Things (IoT) focused on implantable medical devices that can communicate wirelessly for various health monitoring and therapeutic purposes [3]. These devices include pacemakers, glucose monitors, cochlear implants, and neurostimulators. The role of IoIT is to enhance patient care by providing continuous monitoring, real-time data, and improved medical intervention capabilities. With the continuous development of technologies including human-computer interfaces, artificial intelligence, and Micro-Electromechanical Systems (MEMS) [4], the concept of Digital Humans has been recognized as one of the emerging technology fields for the next decade, and implantable devices are certainly one of the key enabling factors in achieving this concept [5]. The advancements of medical implants have been transforming healthcare delivery. These devices are designed to replace, support, or enhance a biological function in the human body. They are used to treat a wide range of medical conditions such as cardiovascular diseases, neurological disorders, hearing loss, and diabetes [6]. Medical implants play a crucial role in improving the quality of life for patients, enabling them to perform daily activities with ease, and reducing the healthcare costs associated with prolonged hospitalization [7].

However, medical implants come with several challenges, one of which is the issue of power supply [8]. Most medical implants require a source of power to operate, and this poses a significant challenge due to the limited lifespan of the batteries used. Implants such as pacemakers, cochlear implants, and insulin pumps need a constant power supply to function correctly [6]. Therefore, power supply is critical to the proper functioning of these medical implants, and any disruption can have severe consequences. There are several factors to consider when selecting a power supply for medical implants. One of the most important factors is the type of implant and the amount of power it requires. Implants such as pacemakers and defibrillators require a high amount of power to operate, while others such as glucose sensors require much less. The type of battery used in the implant also affects the lifespan and reliability of the implant. Lithium-ion batteries are commonly used in medical implants due to their long lifespan and high energy density [9]. However, one of the primary challenges associated with batteries is that they occupy a large percentage of the devices overall volume and require regular replacement. Another issue with battery-powered implants is that they can be difficult to recharge. This is especially true for devices that are implanted deep within the body, such as pacemakers. In

some cases, patients may need to undergo surgery to replace the battery [10], which can be risky and may require a long recovery period.

To address these issues, researchers are exploring alternative power sources for medical implants. One promising approach is energy harvesting. This approach involves converting ambient energy from the surrounding environment, such as body heat or motion, into electrical power. This technology has the potential to provide a continuous source of power for implants, eliminating the need for batteries and external power sources [11], [12]. However, due to the randomness of surrounding energy sources and limited space for energy harvesting devices, this technology faces many challenges in providing sufficient power to some power-demanding or sensing-critical applications. Another promising technology for powering medical implants is the use of wireless power transfer (WPT) technology. WPT allows power to be transferred wirelessly to the implant, eliminating the need for batteries and the costs associated with replacement surgery [13]. A typical type of this technology is transmitting energy through an electromagnetic field from an external power source to the implant. The implant is equipped with a receiver coil that converts the electromagnetic energy into electrical power, which can then be used to operate the device.

However, electromagnetic power transfer also faces challenges in heat generation in human tissues due to ohmic heating characterized by the specific absorption rate (SAR). This is due to high operating frequencies, short power transfer distance, device miniaturization and low transfer power limit according to the U.S. Food and Drug Administration [14]. To address the challenges in effective power transfer over long distances, this paper proposes a new wireless power transfer solution using Halbach array-based magnetic plucking and piezoelectric transduction working at low frequencies for the first time, to the best of the authors' knowledge. The major contributions of this work includes:

- The establishment of a new extended-range wireless power transfer methodology using transcutaneous Halbach-Array-based magnetic plucking and piezoelectric transduction.
- A fully coupled magnetic-piezoelectric-electromechanical model to study the dynamics of the system.
- A miniaturized prototype including a wearable rotating Halbach array coupled with a piezoelectric receiver to illustrate the effectiveness of the new WPT method.

The remainder of this article is organized as follows. The related literature is reviewed in Section II. Sections III describes the proposed approach, its theoretical model and the numerical analysis of the WPT system. Section IV presents the prototyping and experimental validation, followed by a conclusion in Section V.

II. RELATED WORK

Different mechanisms have been adopted in WPT for implantable devices including electrostatic, inductive, ultrasonic and optical power transfer methods [15], [16], [17]. Among them, inductive power transfer receives the most significant attention due to its simplicity in design and high power transfer capability [18], [19]. It involves the transfer of electrical energy between two coils, namely the primary coil outside the body and the secondary coil inside the body. The efficiency and power transfer distance in implantable devices depends on various factors, including the size of the coils, the frequency of the current and the alignment between the transmitter and receiver coils [20].

Shah and Yoo studied the influence of biomedical implants in an electric vehicle charging scenario on body tempature due to the heat generated by WPT, and concluded that with the SAR scaled to a power of 1 W, the steady-state temperature enhancement of some tissues was significantly higher compared to the absence of the implant at the same location [21]. Kim et al. developed a WPT solution for implants by reducing the equivalent series resistance of the transmitting coil and adding a ferrite film to the receiver [22]. To address the misalignment issue, Qian et al. studied a 3-D through silicon via based orthogonal receiving coil to enhance the inductive coupling between coils under misalignment [23]. Wang et al. proposed an array of four identical coils surrounded by a larger coil to generate uniform magnetic field, and the testing results illustrates a high power transfer efficiency even under 1 cm lateral misalignment [24].

Ultrasonic (acoustic) power transfer (UPT) using piezoelectric [25], capacitive [26] or triboelectric transducers [27] is another emerging method to deliver power to implantable devices. Compared to the receiving coils used in inductive power transfer, piezoelectric or capacitive receivers are more compact and lightweight, which is ideal for miniaturized implantable devices [28]. In addition, piezoelectric transducers are capable of operating over a wider frequency range from a few Hertz up to several Megahertz compared to conventional electrical effect based devices. Due to the reduced body heat generated by ultrasonic or acoustic waves, UPT normally has a higher power safety limit than IPT. All these reasons facilites the swift growth of this area. Hong et al. fabricated a wood-templated unidirectional piezoelectric composite for ultrasonic wireless power transfer with an average output power density of 304 μW/cm^2 [29].

Another emerging technology developed alongside WPT is simultaneous wireless power and data transfer, which typically uses the same transducers for both power transfer and data communication functions [30]. The integration of power and data transfer in the same transducer allows for reduced implant size and power consumption for data communication [31]. Najjarzadegan et al. developed an open-loop double-carrier simultaneous wireless power and data transfer system based on the inductive coupling method [32]. Sonmezoglu et al. built a millimeter-sized, wireless, ultrasound-powered implantable luminescence O$_2$ sensor and an external transceiver for bidirectional data transfer, enabling deep-tissue oxygenation monitoring for surgical or critical care indications [33].

Although significant progress has been achieved in WPT for implantable devices, there are still many challenges in bio-compatibility [34], [35], device miniaturization [36], [37], tissue heat generation [38], [39] and WPT for implants located deep within the body [40], [41]. In this study, a new magnetic

coupling based WPT methodology is proposed to deliver sufficient power over a large distance at low frequencies in a miniature wearable-implantable system using a novel magnetic plucking method implemented by a rotating wearable magnetic array and an implanted piezoelectric receiver.

III. PROPOSED MAGNETIC WPT METHODOLOGY AND ASSOCIATED THEORETICAL MODEL

A. Magnetic WPT Method

The WPT solution includes a wearable power transmitter and an implantable piezoelectric receiver, as shown in Fig. 1(a). The coupling between the wearable and implantable devices is established by the magnetic field between the tip magnet on the piezoelectric receiver and a magnetic array on the wearable device, as shown in Fig. 1(b) and (c). In order to excite the piezoelectric beam, the magnetic array has to be in motion relative to the tip magnet on the implant. Therefore, the wearable magnetic array can be either driven passively by human motion using structures such as an pendulum to acquire energy from human motion or actively using a motor.

To deliver power to the implants reliably and reduce the size of the wearable device, a miniature motor with a circular rack and pinion gear system is adopted, as shown in Fig. 1(c). The oscillating magnetic field produces an alternating magnetic force on the tip magnet of the piezoelectric beam, generating a voltage via the piezoelectric effect, and realizing WPT to the implant. In order to increase the power transfer distance, a special type of magnetic array, i.e. a Halbach array, is employed in this study to create an enhanced magnetic field in the direction where the implant is located. A Halbach array is a special type of magnetic array whereby the magnetic field on one side is enhanced by arranging magnets in a specific pattern by alternating the magnetization direction in two directions, as shown in Fig. 1(d), which differs from a typical alternating array (Fig. 1(e)) used in many studies within the literature.

In a Halbach array, the orientation of the magnets is carefully arranged to produce a strong magnetic field pattern on one side while cancelling out the field on the other side. The magnets with the magnetization direction pointing in the vertical direction are named as main magnets, and the others are called transit magnets, as shown in Fig. 1(d). The magnets are arranged so that the north and south poles of the magnetic field all face the same direction on one side of the array, while on the other side, they face in the opposite direction. This creates a strong and uniform magnetic field on the side where the north and south poles combine in the same direction, while the field on the weak side cancels to near zero. This electrodynamic WPT mechanism using the Halbach array, magnetic plucking and piezoelectric transduction is advantageous for wearable-implantable applications given its low operating frequency, device miniaturization and high durability.

The non-contact mechanism of this WPT method has the advantage of increased longevity due to reduced material degradation. The low-frequency operation offers several advantages. The comparatively slow-varying magnetic field (less than 1 kHz) generated by the the rotating permanent magnets can penetrate various non-magnetic materials, including conductive bio-tissues and implant-grade stainless steel housing

without significant loss. The low frequency range ensures that electromagnetic field exposure remains at a non-thermal level, significantly reducing absorption by biological tissue. Piezoelectric devices are particularly suitable for application in medical devices where precision, sensitivity and robustness are critical. Compared to purely electrical effect based devices, piezoelectric transducers have a higher sensitivity and can detect very small changes in force. They output high voltages from relatively small mechanical displacements making them an energy dense alternative to conventional electrical actuators.
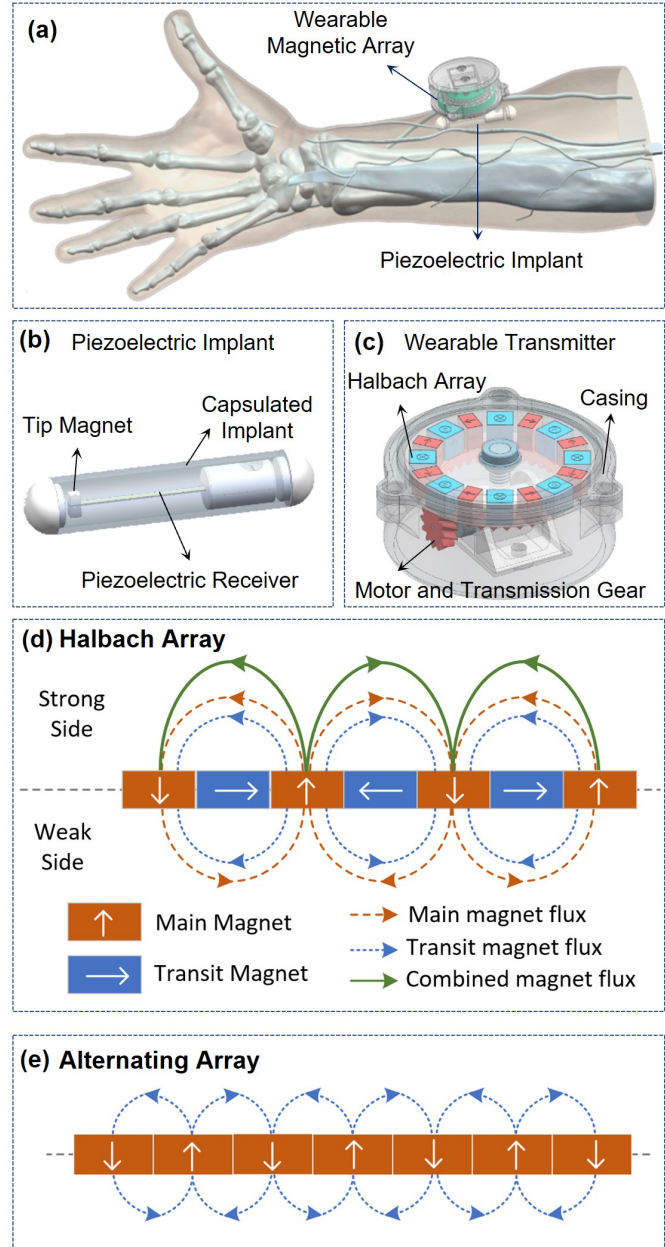

Fig. 1. Operating principle of the transcutaneous WPT technique using piezoelectric transduction and magnetic plucking in a wearable-implant-coupled system. (a) Schematic of the location and configuration of the wearable and implantable devices; (b) Implanted piezoelectric receiver; (c) Wearable rotating Halbach array driven by a miniature motor; (d) Magnet arrangement pattern and associated magnetic field distribution of Halbach array; and (e) typical alternating array as a reference.

By enabling the seamless powering of medical implants and wearable devices, this WPT technology can enhance patient outcomes through continuous monitoring and treatment. For instance, cardiac pacemakers and insulin pumps could benefit from wireless power, reducing the need for frequent battery replacement and invasive procedures. This not only improves patient comfort and compliance but also decreases the risk of complications and infections. Overall, integrating wireless power transfer in healthcare can lead to more efficient, reliable, and patient-friendly medical solutions, ultimately transforming patient care and improving quality of life.

B. Theoretical Modelling

The theoretical model is an essential tool to analyse the electro-magneto-mechanical dynamic response of the system. In addition, when enhancing the performance of the WTP solution, it is necessary to evaluate different design parameters to maximise the strength of the magnetic field and the delivered power. A theoretical model is therefore indispensable when considering the design of the transmitter and receiver. This theoretical model includes the magnetic coupling between the Halbach array and the tip magnet, and the electromechanical model of the piezoelectric transducer in a coupled manner.

1) Magnetic Coupling: Fig. 2(a) shows the magnetic coupling between the wearable Halbach array driving magnets and the implanted receiver tip magnet. Two cases have been considered for a Halbach array magnetisation pattern. For Case ① in Fig. 2(a), the driving and tip magnets are both magnetised in the z-axis direction. For Case ②, the magnetisation of the transit magnets are orientated perpendicularly to the tip magnet.

In order to model the magnetic coupling force exerted by the magnets of the Halbach array on the tip magnets attached to the piezoelectric beam, the theory developed by Yonnet *et al.* [42], [43] has been adopted. For two cuboidal magnets, the magnetic force from the ith Halbach array magnet in the direction of beam vibration (z axis component) can be expressed as [42]

$$F_i^z = \frac{J_1 \cdot J_2}{4\pi\mu_0} \sum_{i=0}^{1}\sum_{j=0}^{1}\sum_{k=0}^{1}\sum_{l=0}^{1}\sum_{p=0}^{1}\sum_{q=0}^{1}(-1)^{i+j+k+l+p+q} \cdot \phi_z^d \tag{1}$$

where J_1 and J_2 are magnetic remanence values of the tip and array magnets respectively, μ_0 is the magnetic constant, i, j, k, l, p, n are the indices of different corners of the cubic magnets, and ϕ_z^d is a function of the magnet dimensions and the relative positioning of the tip and array magnets for different magnetisation directions, with d being either parallel or perpendicular to the magnetisation direction of the tip magnet. The summation terms in Eq. 1 was derived from the integration expression of the forcing term, and the whole derivation can be found in Ref. [42]. This simplification makes this equation easier to be used in numerical calculations without compromising the accuracy. The validation of this equation has been done by previous studies [43], [44].

In the parallel condition, the function is given by

$$\phi_z^{\parallel} = -U_{ij}W_{pq}(r - U_{ij}) - V_{kl}W_{pq}\ln(r - V_{kl}) \\ + U_{ij}V_{kl}\left(\frac{U_{ij}V_{kl}}{W_{pq}r}\right) - W_{pq}r \tag{2}$$

For the perpendicular magnetisation direction condition, the function becomes

$$\phi_z^{\perp} = \frac{(U_{ij}^2 - W_{pq}^2)}{2}\ln(r + V_{kl}) - U_{ij}V_{kl}\ln(r - U_{ij}) \\ - U_{ij}W_{pq}\left(\frac{U_{ij}V_{kl}}{W_{pq}r}\right) - \frac{1}{2}V_{kl}r \tag{3}$$

where U_{ij}, V_{kl} and W_{pq} are intermediary variables that define the distance between the corners of each Halbach magnet to their respective projection in each axis and r being the magnitude of these components. The expressions for these intermediary variables can be found in the appendix. The total magnetic force exerted on the tip magnet is calculated by

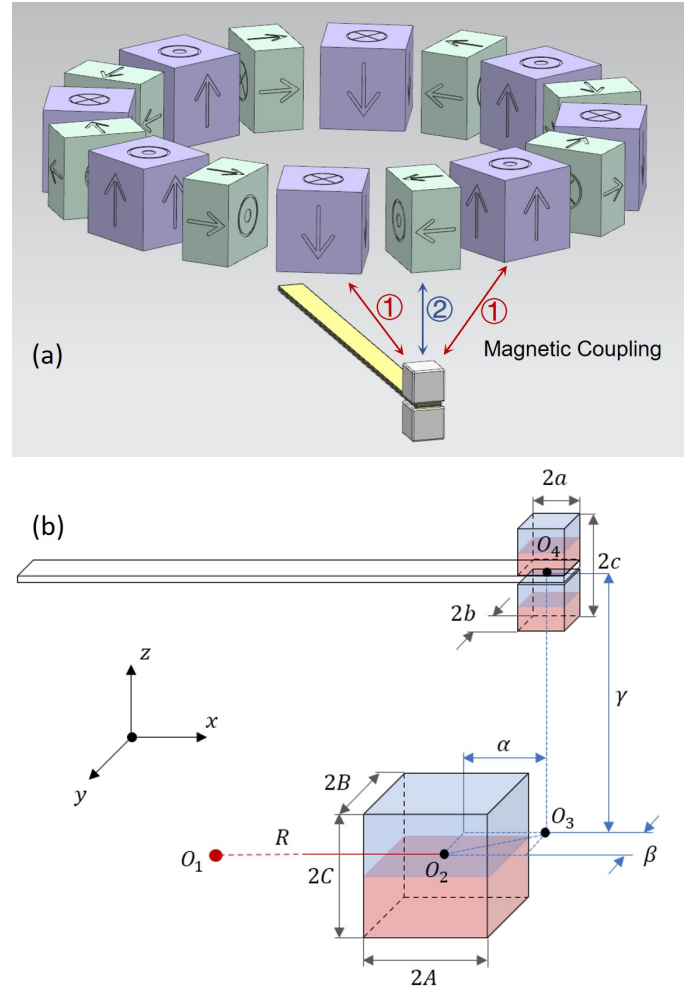$$F_s^z = \sum_{i=1}^{n}(-1)^{floor\left(\frac{n}{2}\right)}F_i^z \tag{4}$$

Fig. 2. Magnetic coupling between the Halbach array and the tip magnetic on the piezoelectric receiver. (a) Halbach array and tip magnet configuration and (b) Relative dimensions of one magnet in the array relative to the tip magnet of the implanted receiver.

where the function $floor(x)$, which generates the greatest integer less than or equal to x, has been used to reverse the polarity condition of the magnets.

2) Piezoelectric Transducer: The piezoelectric receiver in Fig. 1(b) can be modelled as a cantilever beam with a tip mass. Using a distributed-parameter method developed by Erturk and Inman [45], the dynamics of the beam can be modeled as

$$YI\frac{\partial^4 \upsilon(x,t)}{\partial x^4} + c_s I\frac{\partial^5 \upsilon(x,t)}{\partial x^4 \partial t} + c_d\frac{\partial \upsilon(x,t)}{\partial t} + m\frac{\partial^2 \upsilon(x,t)}{\partial t^2}$$
$$-\vartheta V(t)\left[\frac{d\delta(x)}{dx} - \frac{d\delta(x-L)}{dx}\right] = F_{mag}^z \quad (5)$$

and

$$\frac{C_p}{2}\frac{dV(t)}{dt} + \frac{V(t)}{R_l} + \bar{e}_{31}\frac{h_p + h_s}{2}b\int_0^L \frac{\partial^3 \upsilon(x,t)}{\partial x^2 \partial t}dx = 0 \quad (6)$$

where YI is the bending stiffness of a composite piezoelectric bimorph, $c_s I$ is the internal damping, c_d is the viscous damping, m is the mass per unit length of the beam, ϑ is the piezoelectric coupling term in physical coordinates, $V(t)$ is the voltage across the resistive load R_l, $\delta(x)$ is the Dirac delta function, C_p is the inherent capacitance of the piezoelectric beam, $\bar{e_{31}}$ is the piezoelectric constant, h_p is the height of the piezoelectric layer, h_s is the height of the structural substrate layer, b is the beam width and L is the length of the beam. The displacement of the beam, $\upsilon(x,t)$ can be expressed as the mode superposition of N modes participation:

$$\upsilon(x,t) = \sum_{r=1}^{N}\phi_r(x)\eta_r(t) \quad (7)$$

where $\phi_r(x)$ the eigenvector of the rth eigenmode of the beam with modal participation factor $\eta_r(t)$. The mechanical equation can be reduced to the equivalent representation for the electromechanical equations governing the modal coordinate and voltage response by substituting Eq. 7 into Eq. 5. Multiplying through by $\phi_r(L)$ and integrating over the length of the beam gives

$$\frac{d^2\eta_r(t)}{dt^2} + 2\zeta_r\omega_r\frac{d\eta_r(t)}{dt} + \omega_r^2\eta_r(t) - \vartheta_r V(t) = F_s^z\phi_r(L) \quad (8)$$

where ζ_r is the modal damping ratio of the rth mode shape and can be obtained experimentally by analyzing the frequency response function data obtained from a ring-down test (impact test). The electrical response of a bimorph can be expressed as

$$C_p\frac{dV(t)}{dt} + \frac{V(t)}{R_l} + \sum_{r=1}^{\infty}\vartheta_r\frac{d\eta_r(t)}{dt} = 0 \quad (9)$$

where C_p is the capacitance for piezoeceramic layers. The coupled magnetic-mechanical-electrical dynamics can be studied by solving Eqs. (4), (8) and (9) in a coupled manner.

IV. NUMERICAL AND PARAMETRIC STUDY

In order to examine the electro-magneto-mechanical dynamics of this wireless power transfer system, a detailed numerical study is presented in this section to illustrate the uniqueness and the advantages of using Halbach arrays and piezoelectric transduction. The numerical results were obtained by solving Eqs. (4-9) using the Runge-Kutta method (i.e. ode45 in Matlab). The time step was set as 1×10^{-5} s to ensure the dynamics of the system can be accurately captured.

A. Magnetic forces from the Halbach array

The magnetic coupling between the tip magnet and the Halbach array establishes the link between the implanted devices and the external wearable device. Therefore, it is critical to understand how different design parameters and arrangements affect the coupling strength. Using the parameters provided in Table I, the magnetic forces can be determined using Eqs. (1)-(4), as shown in Fig. 3.

Fig. 3(a) shows the magnetic force between the tip magnet on the piezoelectric beam and one of the main magnets on the Halbach array, for which the magnetisation direction is the same as that of the tip magnet. This main magnet interacts with the tip magnet once per revolution, and the force is in the form of an impulse. Fig. 3(b) shows the forces for four magnets in a typical Halbach array pattern, namely Mag. 1 (main magnet) - Mag. 2 (transit magnet) - Mag. 3 (main magnet) - Mag. 4 (transit magnet) in a form of chaning polarity, as shown in Fig. 1(d). These forces have distinct distributions due to the variation of the magnetisation directions. Fig. 3(c) depicts all the forces from the magnets in the array and the summation of the forces (black curve). It can be seen that the overall force amplitude is enhanced by 37.2% (18.4/12.1), as shown in Fig. 3(a)-(c).

A direct comparison among the strong side and weak side of the Halbach array and the alternating array is provided, as shown in Fig. 4. The strong side exhibits an enhanced magnetic force due to the strengthening effect, whereas the weak side shows significantly reduced force intensity (0.8 mN vs 3.8 mN), as shown in Fig. 4(a). For the alternating array, the force amplitude is slightly larger than that of the weak side, but

TABLE I
PARAMETERS OF THE COUPLED WEARABLE-IMPLANTABLE WPT SYSTEM.

Symbol	Description	Value
Motor parameters		
r_P	Motor radius	3.5 mm
l_m	Motor length	25 mm
d_g	Gear diameter	13.5 mm
Magnet Parameters		
$a\times b\times c$	Driving magnet size	$1.5 \times 1.5 \times 0.75$ mm
$A\times B\times C$	Tip magnet size	$0.5 \times 0.5 \times 0.5$ mm
h_0	Initial gap in z-axis	5 mm
J	Magnetization of magnets	1.17 T
ρ_m	Density of magnets	7400 kg/m³
Piezoelectric beam parameters		
$L_p \times b_p$	Beam size	25 mm $\times$ 1.5 mm
h_p	Thickness of piezo layer	0.1 mm
h_s	Thickness of substrate	0.1 mm
$\bar{e}_{31}$	Piezoelectric voltage constant	-22.5 V $\cdot$ m/N
d_{31}	Piezoelectric charge constant	-315 m/V
ρ_p	Density of piezoelectric material	7800 kg/m³
ρ_s	Density of substrate material	7850 kg/m³
Y	Young's modulus of substrate	190 GPa
ϵ_{r33}^T	Relative permittivity constant	4500
s_{11}^E	Elastic constant (compliance)	14.2×10^{-12} m²/N

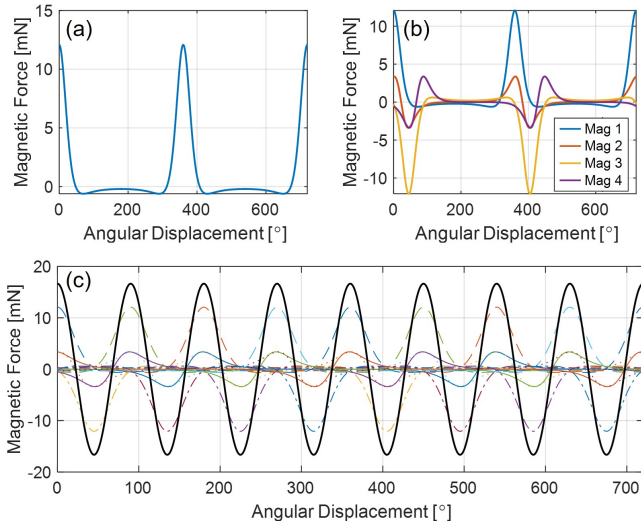is still much smaller than that of the strong side, showing the

Fig. 3.   Magnetic force between the tip magnet and the Halbach array for a 15 mm gap. (a) Magnetic force from one magnet with the magnetisation direction the same as the tip magnet; (b) Forces from four magnets in a typical Halbach array cycle; (c) All individual forces from the array magnets and the overall force (black curve).
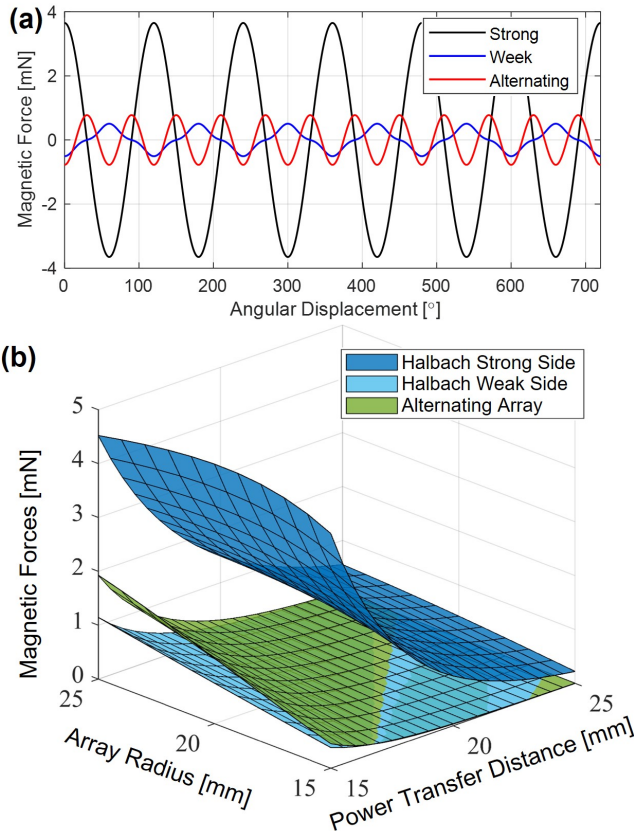

Fig. 4.   Magnetic force comparison of the weak side, strong side and an alternating array. (a) Comparison of three cases with 12 magnets and 15 mm gap, and (b) Magnetic force comparison against array radius and power transfer distance.
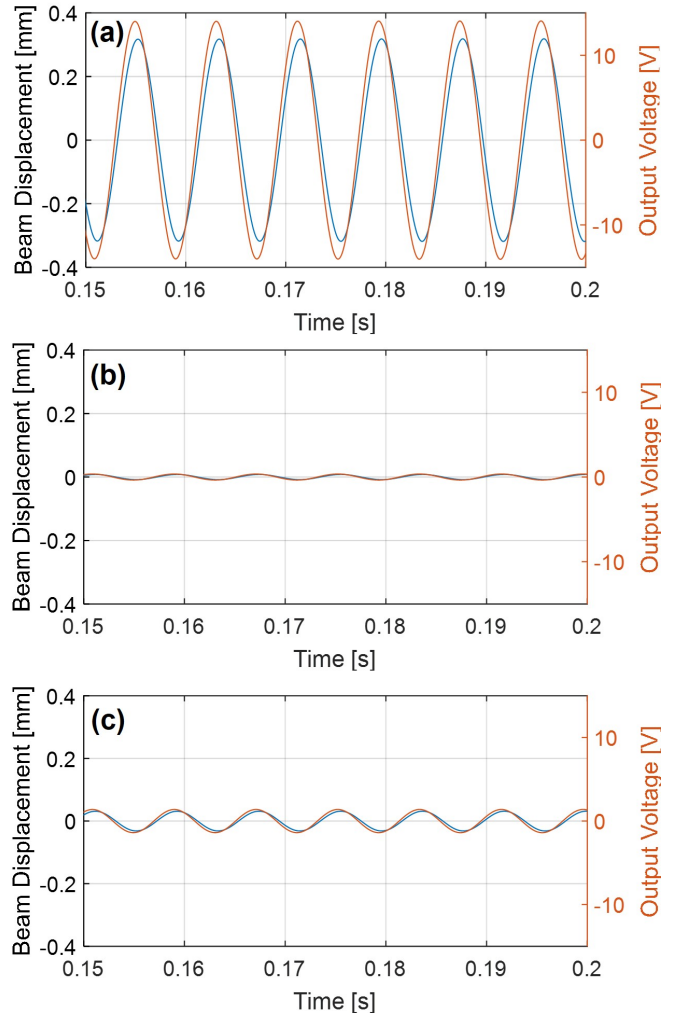

Fig. 5.   Output voltage of the WPT device for different array cases with a 15 mm with the beam vibrating at its natural frequency. (a) Halbach strong side, (b) Halbach weak side and (c) Alternating array.

advantage of using the Halbach array for power transfer over longer distance. It is worth noting that when using the Halbach array, four magnets form a pole pair, whereas two magnets can form a pole pair in the alternating array, as shown in Fig. 1(e). This explains why the frequency of the magnetic force from the alternating array is higher than that of the Halbach array, as shown in Fig. 4(a). Fig. 4(b) illustrates the comparison of the magnetic forces against the array radius and the power transfer distance for the above-mentioned three configurations with the strong side of the Halbach array demonstrating its dominance over the investigated ranges. The weak side of the Halbach array is always the weakest, which is ideal for wearable devices when avoiding any disturbance due to the existing magnetic field, since the weak side of the Halbach array is orientated to face the opposite side to human skin where the users body will have many interactions with outside world.
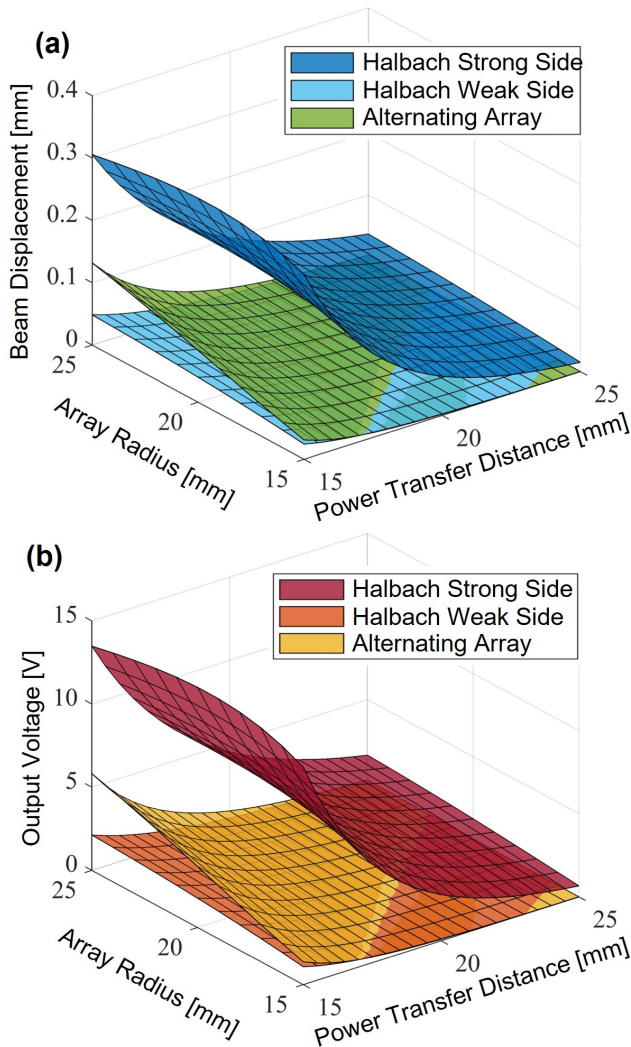
Fig. 6. Beam displacement and output voltage of the WPT device for different array cases against array radius and power transfer distance. (a) Beam displacement and (b) Output voltage.

the beam tip displacement and output voltage variation for different array radii and power transfer distances for the different arrays. The strong side of the Halbach array is configured in the ideal condition for wireless power transfer given the increased displacement and output voltage over the whole range, as expected from the significantly higher generated forces presented in Fig. 4. The alternating array is better in most conditions than the weak side of the Halbach array, but is less effective when the power transfer distance is larger or the array radius is smaller. This is mainly due to the variation of the magnetic field distribution, as the magnetic field will be weakened if the array is not well designed, as shown in Fig. 6(b). Based on this evaluation, it is obvious that the Halbach array design is beneficial when delivering power over longer distances.

These numerical results will be correlated and compared to the experimental results in the following section to validate the theoretical model and the electromechanical dynamics.

V. PROTOTYPING AND EXPERIMENTAL VALIDATION

A. Prototype and Experimental Setup

In order to examine the WPT performance of the proposed magnetic plucking-based solution, a prototype is built as
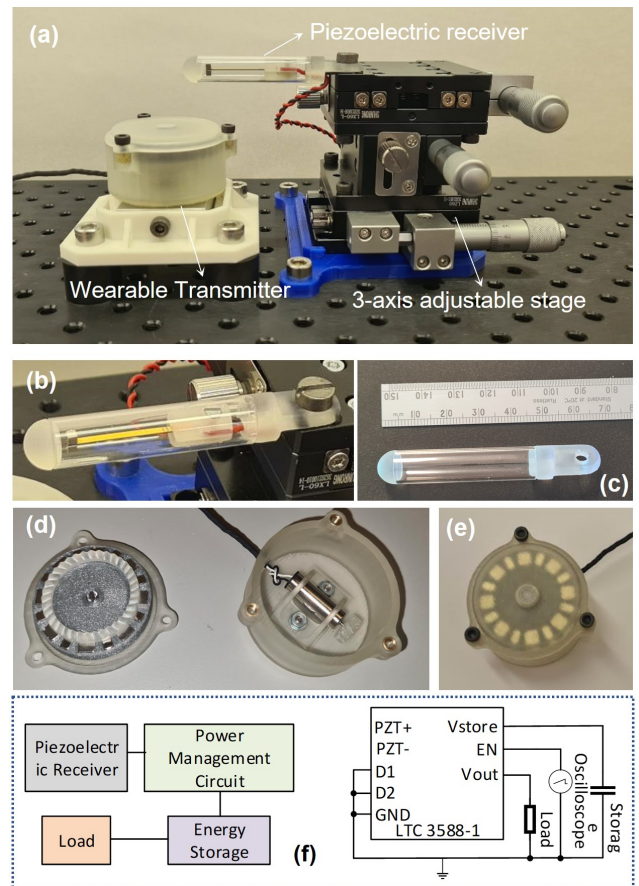

Fig. 7. Transmitter and receiver prototypes and experimental setup of the proposed WPT system. (a) Experimental setup; (b) Encapsulated piezoelectric receiver; (c) Receiver casing with a ruler for comparison; (d) and (e) Wearable transmitter and its components; and (f) Power management circuit for the piezoelectric receiver.

B. Electromechanical dynamics

To further examine the influence of the Halbach array on wireless power transfer, the electromechanical dynamics of the piezoelectric beam under the magnetic force excitation is investigated, as shown in Fig. 5. The beam tip displacement and output voltage changes drastically among three array cases, with the beam displacement and output voltage from the strong side of the Halbach array being the largest. The output voltage amplitudes are 14 V, 0.36 V and 1.4 V, respectively from the strong and weak sides of the Halbach array and the alternating array. To ensure the beam operates at its natural frequency, the rotational frequency of the Halbach array is two times faster than the alternating array at 1/4 of the beam's natural frequency (f_n) when 16 magnets are adopted in the array.

The power transfer distance and array radius also affect the power generation capability of the piezoelectric receiver as a result of the changing magnetic field. Fig. 6 illustrates

shown in Fig. 7. The wearable transmitter is placed on an optical table, and the piezoelectric receiver is mounted on a 3-axis adjustable stage to change the gap between the transmitter and receiver in three directions accurately, as shown in Fig. 7(a). Fig. 7(b) depicts the details of the piezoelectric receiver as a prototype. The piezoelectric beam is mounted in a transparent capsule. The beam is clapped at one end and two cuboidal magnets are mounted at the free end of the beam. Bio-compatibility and miniaturization of the prototype is not the priority of the proof-of-concept stage, but certainly are important aspects to be considered in future studies. The capsule housing features a transparent acrylic tube with two resin printed end caps for the purpose of testing the receiver mechanism within a confined space. Whilst these materials were chosen for convenience and dimensional accuracy during testing, in reality, emerging encapsulation technologies for long-term implants such thin film parylene or polyimide polymer coatings would be required for the capsule housing for their long-term stability in vivo and biocompatibility properties within the human body [46]. In addition to polymer coatings, hydrogel coatings are an established method of minimizing inflammation and fibrosis in the implant site of patients with long term MIDs. For long-term applications, the encapsulation material must exhibit both long-term reliability in aqueous environments, good electrical insulation and offer conformal encapsulation of complex topography for this work to be realized in medical applications. When considering the bio-compatibility of piezoceramics, lead-free piezoceramics can be used to eliminate any adverse health effects that could arise from lead toxicity [47].

Fig. 7(c) shows the dimensions of the capsule. Fig. 7(d) presents the disassembled wearable transmitter. A Halbach array was fabricated and mounted on a circular gear rack, and a miniature DC motor is adopted to drive a pinion. This pinion-and-rack mechanism allows the Halbach array to rotate at a desired speed determined by the resonant frequency of the piezoelectric receiver. The transmitter casing was manufactured using stereolithography with a lightweight resin for its high dimensional accuracy. The housing incorporates an affordable miniature DC motor, selected for its compact size and low power consumption, which drives the Halbach array using a rack and pinion gear system. For comfort, the wearable device features a flat surface that rests parallel to the owner's skin, providing a comfortable fit similar to that of a wristwatch.

Fig. 7(e) shows the assembled wearable transmitter. A power management and storage circuit is also required to rectify the alternating current (AC) output from the piezoelectric receiver to a stable voltage range suitable for electronics. Fig. 7(f) provides a solution for power management using a commercial solution LTC 3588-1 to rectify the output voltage suitable for implantable electronics.

B. Experimental Validation

The theoretical model provides a convenient way to efficiently study the electromechanical dynamics, but the validity of the model also needs to be evaluated. Modal analysis tests under impulse excitation were carried out to compare the

experimentally obtained resonant frequency to the theoretical value output by the model. The modal analysis was performed with impulse excitation to a plane normal to the PZT beam in order to measure the bending modal frequencies, as shown in Fig. 8(a). The beam plectrum can be manually moved upwards or downwards accurately by a 3-axis optical stage. The beam can be deflected by moving the stage upwards or downwards when the plectrum is in contact with the piezoelectric receiver. After being deflected, the piezoelectric receiver can be released by moving the plectrum swiftly in the horizontal plane using the 3-axis optical stage. After being released, the beam response under the impulse excitation can be measured using the oscilloscope to obtain the resonant frequencies of the piezoelectric receiver.

Fig. 8(b) demonstrates the measured free vibration time response of the beam magnet in the normal direction under impulse excitation, while Fig. 8(c) presents the frequency content of the time response. From the measurements, it is clear that 2 bending modal frequencies exist in the frequency range up to 500 Hz with the dominant 1st bending mode existing at 121 Hz, as shown in Fig. 8(c).

To validate the theoretical model, Table II provides the comparison of the resonant frequencies obtained by the theoretical model and the experimental tests, respectively. A close match is obtained (less than 5% of resonance frequency difference between the theoretical results and the numerical results, 2.36% in average), showing the capability and validity of the theoretical model. It is clear from Table II that there are two parameters that drastically affect the beam modal frequencies, the free beam length and the concentrated mass. So according to the application and the system requirements tuning of these two parameters can shift the piezoelectric beam modal frequencies to the appropriate frequency increasing the
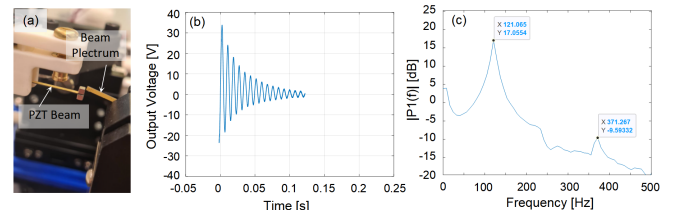

Fig. 8. Piezoelectric receiver impulse excitation test using the beam plucking method. (a) Plucking experimental set-up, (b) Output voltage response under beam impulse excitation, and (c) Frequency response function (FRF) of the impulse excitation, showing the resonant frequency.

TABLE II
PIEZOELECTRIC BEAM RESONANT FREQUENCY VALIDATION USING
IMPULSE EXCITATION TESTS

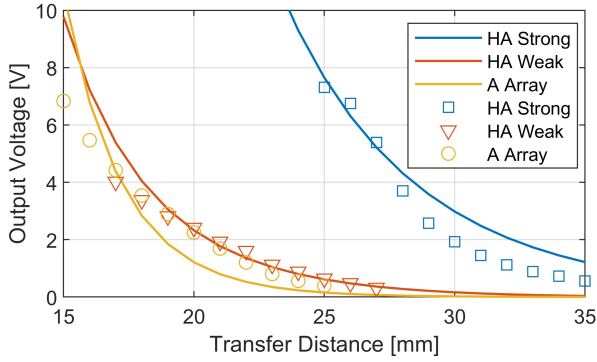| Effective Length	Theoretical Model Frequency	FRF Peak Frequency	Difference
Beam without tip mass			
24 mm	286.4 Hz	280.0 Hz	2.25%
22 mm	340.84 Hz	330.0 Hz	3.23%
20 mm	412.4 Hz	400.0 Hz	3.05%
18 mm	509.1 Hz	535.0 Hz	4.96%
16 mm	644.4 Hz	630.0 Hz	2.25%
Beam With tip mass			
23 mm	95.06 Hz	96.78 Hz	1.79%
22 mm	102.58 Hz	102.83 Hz	0.24%
21 mm	111.10 Hz	110.89 Hz	0.19%
20 mm	120.80 Hz	116.94 Hz	3.25%

Fig. 9. Numerical and experimental comparison of the implanted receiver output voltage for different transmitter configurations. The solid lines represent the numerical study, and the markers show the experimental results (HA - Halbach Array; A Array - Alternating Array).

Fig. 10. Frequency sweep test of the harvester for different array arrangements to show the resonant frequency and output voltages.

efficiency for a specific Halbach array rotation speed.

C. Output Performance

Using the experimental setup in Fig. 7(a), the power transfer distance for different array arrangements is studied to examine the wireless power transfer capability, as shown in Fig. 9. In the experimental study, the gap between the transmitter and receiver is adjusted for different configurations to avoid extensive magnetic force being applied to the piezoelectric beam, with the output voltage confined to within 10 V. The strong side of the Halbach Array is advantageous in transferring the power over longer distances (25 mm to 30 mm), producing more than 2 V on the receiving piezoelectric beam (Fig. 9). For the weak side of the Halbach Array and the standard alternating array, the magnetic fields attenuate drastically within a short distance from 15 mm to 20 mm, and the receiver's output voltage is less than 2 V.

The comparison between the numerical and experimental results are further compared to show the validity of the theoretical model. A close match has been obtained, as shown in Fig. 9. The theoretical model can accurately predict the trend of the output voltage for different transfer distances and different array configurations. The minor differences between the numerical and experimental results are mainly due to the discrepancy of magnetic material parameters and structural dimensions used in the experimental and numerical studies.

The frequency response of the piezoelectric receiver is studied by applying rotational motion with different frequencies to each wearable magnetic array configuration. The output voltage of the piezoelectric receiver under different excitation frequencies is shown in Fig. 10. The rotational frequency ranges from 0 to 37 Hz. As shown in Fig. 10, the piezoelectric receiver reaches resonance at around 17 Hz (6 pole pairs, 17×6=102 Hz), 32 Hz (3 pole pairs, 32×3=96 Hz) and 34 Hz (3 pole pairs, 34×3=102 Hz) for different array configurations, respectively. The natural frequency for this beam is around 102 Hz. The strong side exhibits a slight change in the driving frequency due to the variation of the magnetic field distribution. For the alternating array, the piezoelectric receiver
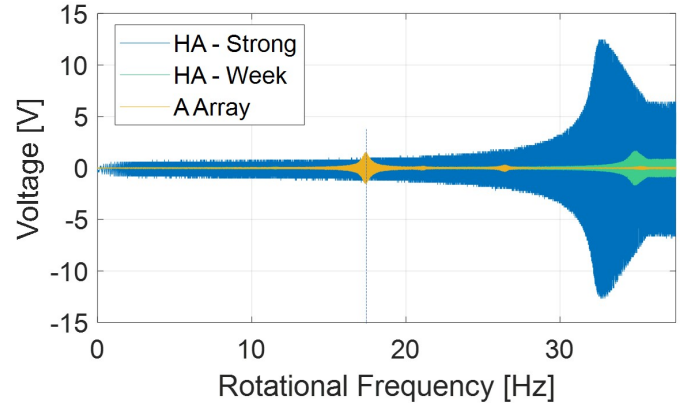
reaches resonance at around 17 Hz (rather than 34 Hz) due to the doubled number of pole pairs compared to the Halbach Array, as shown in Fig. 1(d). The output voltage of the receiver excited by the strong side of the Halbach Array exhibits the best performance in wireless power transfer with a peak voltage of over 10 V.

D. Influence of Environmental Conditions

Environmental variations such as temperature and humidity may change the performance of the system. The mechanical durability of the system is critical for long-term application of such implantable devices and therefore, the system's durability and environmental dependability have been examined, as shown in Fig. 11. Fig. 11(a) depicts the output voltage of the piezoelectric receiver under continuous excitation from the wearable device for 32 mins (more than 100k cycles). The details of the output voltage is enlarged as shown in Fig. 11(b). It can be seen that the output voltage is stable over the whole duration without noticeable degradation.

The influence of temperature and humidity variation has also been examined using an environmental chamber (ES-PEC EW0470, China), as shown in Fig. 11(c) and (d). The humidity variation is tested between 40% to 90%, based on the typical conditions of wearable and implantable devices. This experiment was conducted by changing the humidity levels to a certain value and measuring the output voltage for 50 s after the humidity level stabilized. The forward and backward testing results for different humidity levels are shown in Fig. 11(c). The output voltage reduces as the humidity increases, however the performance can be recovered if the humidity level returns to its original value. The variation in output voltage could be due to the change in the material properties or a shift in the resonant frequency point. The variation of temperature has similar influence on the output voltage, as shown in Fig. 11(d). Again, this influence can also be recovered if the temperature returns to the original value. For a receiver implanted inside the human body, the actual variation of temperature and humidity will be marginal, especially when the receiver is well encapsulated.
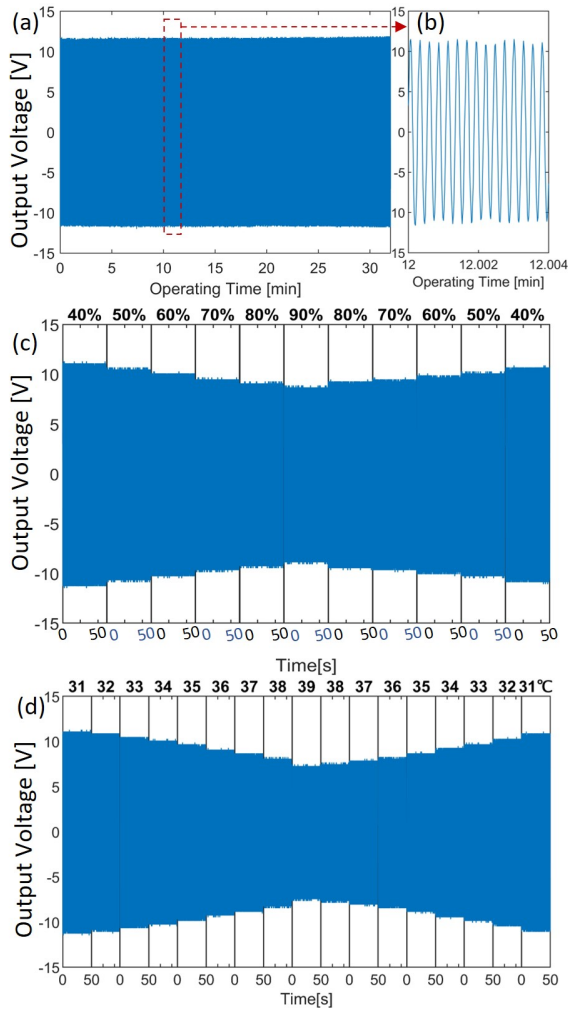
Fig. 11. Evaluation of the influence of the environmental factors: (a) Mechanical durability over 30 minutes, (b) Enlarged section of the mechanical durability test, (c) Relative humidity (40% - 90%) and (d) Temperature (31 °C - 39 °C). Each temperature and humidity condition was stabilized before each 50 second test. The plots were combined afterwards.
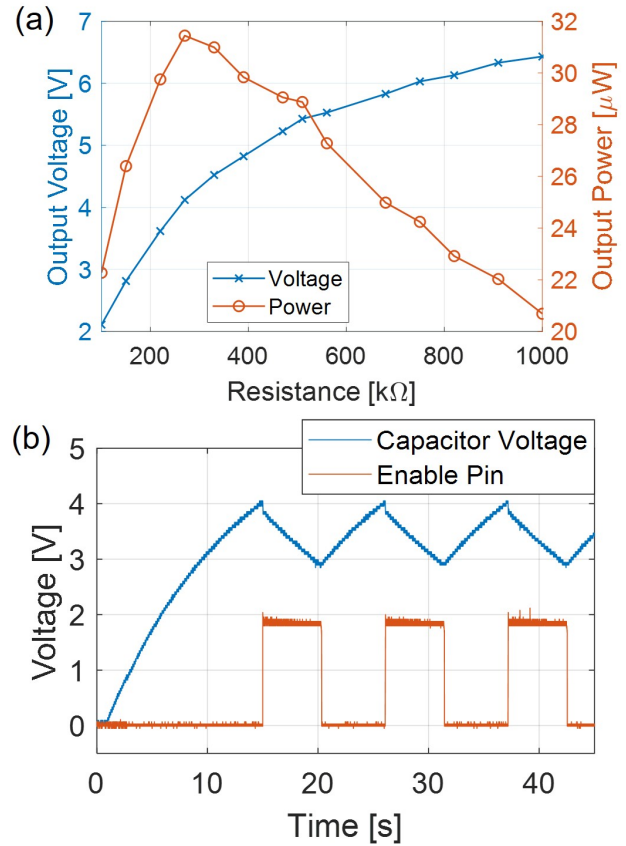

Fig. 12. Output power and self-powered sensing ability testing: (a) Impedance matching test for a 22 mm air gap and (b) Autonomous charging and discharging capability for the receiver connected to a 22 μF capacitor and a 150 kΩ resistive load.

E. Performance Comparison

In order to show the advantage and the uniqueness of this developed solution, a comparison table has been created to compare the performance of this work with the related studies in the literature, as shown in Table III. This electrodynamic WPT method with a Halbach Array and piezoelectric transduction in this work is a unique method compared to the literature. In terms of the advantage of this work compared to the related studies in the literature, the dimensions for the transmitter and the receiver are the most appropriate configuration for wearable-implantable devices in healthcare applications operated at relatively low frequencies. The output power from Ref. [48] is the highest in this comparison table, but the dimensions of both the transmitter and the receiver are not appropriate for implantable and wearable devices.

F. Self-Sustained Operation

The performance of the WPT method was further examined for self-sustained operation. The output voltage and power for different resistive loads were evaluated to show the impedance of the receiver for a 22 mm air gap, as shown in Fig. 12(a). Around 31.5 μW of output power is obtained for a 270 kΩ resistive load. Then, the WPT system was combined with the power management circuits in Fig. 7(f) to demonstrate the self-sustained operation capability. An energy storage capacitor (22 μF) with a 150 kΩ load were used to store the energy and to mimic some sensing functions as a load, respectively. The system is capable of cold-start, as shown at the beginning of the charging curve in Fig. 12(b). The charging and discharging cycles can be precisely controlled given the merit of the power management circuit. The enable-pin signal, which indicates if the voltage on the storage capacitor is sufficient or not, can be used as a trigger source for potential sensing applications, such as periodically monitoring of glucose levels inside the human body using event-triggered mechanisms.

Given the achievable useful power output of the wireless power link after the power management circuit, this wireless power transfer (WPT) technique could be applied to medically implanted devices in the μW power range such as biosensors, pacemakers, neuro-stimulators, and cardiac defibrillators [54]. The power consumption of these above-mentioned medical devices is normally between the μW and mW range [55], which can be covered by the proposed WPT method in this work for self-sustained long-term operation. The integration

TABLE III
PERFORMANCE COMPARISON OF THIS WORK AGAINST THE LITERATURE

Author & Year	Transmission Method[1]	Frequency [Hz]	Transmitter Size [cm][2]	Receiver Size	Transfer Distance	Power [mW]
Bhamra et al. & 2017[17]	2.4 GHz ISM Band	434 MHz	–	0.38×10^{-3} cm^3	0.5-1 cm	0.05
Knecht and Kolar & 2019 [20]	IPT Coil pairs	6.85 MHz	–	10.3 (Ø7) cm^3	1 cm	5 W
Ameye et al. & 2023 [48]	EWPT Single Tx coil	45	Ø30 × 4.8	71.7 cm^3	7.5 cm	19
Truong et al. & 2020 [49]	Symmetrical Helmholtz coils	70.5	Ø15.6 × 1.16	0.35 cm^3	3 cm	4.9
Crasto et al. & 2024 [50]	EWPT Singl coil	144	Ø30 × 1.7	53 cm^3	30 cm	975
Halim et al. & 2021 [51]	EWPT	724	Ø15 × 1.5	0.08 cm^3	1 cm	0.36
Smith et al. & 2021 [52]	EWPT Helmholtz coils	735	Ø28 × 3.5	0.09 cm^3	4 cm	0.52
Wu et al. & 2022 [53]	External rotating magnets	55	Ø3 × 4	3.77 cm^3	–	130
This work	EWPT Halbach Array	121	Ø5 × 2.7	0.13 cm^3	2.2 cm	0.032

[1] EWPT - Electrodynamic Wireless Power Transfer; IPT - Inductive Power Transfer.
[2] Some of the dimensions are estimated from the literature.

of this WPT systems with current medical implantable technologies is a promising area of study. This technology could revolutionize how implants are powered, reducing the need for frequent surgeries and enhancing patient comfort. By incorporating WPT into existing medical IoT infrastructure, we can streamline the process and ensure safer, more reliable power delivery to devices like pacemakers and neurostimulators. This integration could significantly improve patient outcomes and quality of life while also paving the way for future advancements in medical technology.

VI. CONCLUSION

In summary, this paper addresses the challenges of transmitting power from a wearable device to an implantable devices via a large gap at low frequencies. A new wireless power transfer method using Halbach-Array-based magnetic plucking and piezoelectric transduction is presented, which is not only ideal for low plucking frequencies, but also easy to integrate in miniaturized devices. This new WPT method delivers around 32 µW of power to the implanted receiver over 22 mm with 37.2% enhancement in magnetic field, illustrating its potential in realizing self-sustained implantable devices.

A comprehensive theoretical model is established, including the magnetic Halbach array, piezoelectric transduction and the electromechanical dynamics. Key parameters, such as the array radius and the power transfer distance, were examined to understand the WPT capabilities and to optimize the system performance. A WPT prototype including the wearable transmitter and the implantable receiver was fabricated and tested. The theoretical model and numerical results are further validated by the experimental results which show a close agreement. The advantage of using Halbach arrays to deliver power over longer distances is illustrated. The self-sustained operation capability is also demonstrated by combining the WPT system with a power management and storage circuit. Future work includes the enhancement of the power delivery ability, enabling simultaneous power and data

transfer, improving the bio-compatibility and further device miniaturization, to promote the realization of personalized and remote healthcare. In terms of the wearable transmitters, features including lightweight, miniaturization, comfort and low-power consumption are critical factors to be considered for use of such devices in practice.

APPENDIX

Some supporting equations are listed in this appendix to reduce the size of the main body of the paper. The variables U_{ij}, V_{kl}, W_{pq} and r to describe the dimension-associated relations in Eqs. (2) and (3) can be expressed as:

$$U_{ij} = \alpha + (-1)^j A - (-1)^i a \tag{10}$$

$$V_{kl} = \beta + (-1)^l B - (-1)^k b \tag{11}$$

$$W_{pq} = \gamma + (-1)^q C - (-1)^p c \tag{12}$$

$$r = \sqrt{U_{ij}^2 + V_{kl}^2 + W_{pq}^2} \tag{13}$$

where A, B, C, a, b and c refer to the half dimensions of the array and tip magnet respectively whilst α, β and γ are the relative displacements between the magnets in the x, y and z axis respectively. For an Halbach array operating at a rotational frequency of ω, equations of circular motion have been utilised to calculate α, β and γ as follows

$$\alpha_i = R - \left(R \cos \left(\omega t - 2\pi \frac{i-1}{n} \right) \right) \tag{14}$$

$$\beta_i = R \sin \left(\omega t - 2\pi \frac{i-1}{n} \right) \tag{15}$$

$$\gamma_i = |O_3 O_4| + z_i \tag{16}$$

$$R = |O_1 O_2| \tag{17}$$

where n is the number of Halbach array magnets and i (= 1, 2, 3, ... n) is the ith Halbach array magnet and R is the radius of the Halbach array from the centre of rotation to the magnet centres.

ACKNOWLEDGMENT

REFERENCES

[1] M. Roudneshin, K. Sayrafian, and A. G. Aghdam, "Adaptive maximization of the harvested power for wearable or implantable sensors with coulomb force parametric generators," *IEEE Internet of Things Journal*, 2023.

[2] R. Singh, M. J. Bathaei, E. Istif, and L. Beker, "A review of bioresorbable implantable medical devices: Materials, fabrication, and implementation," *Advanced Healthcare Materials*, vol. 9, no. 18, p. 2000790, 2020.

[3] G. E. Santagati, N. Dave, and T. Melodia, "Design and performance evaluation of an implantable ultrasonic networking platform for the internet of medical things," *IEEE/ACM Transactions on Networking*, vol. 28, no. 1, pp. 29–42, 2020.

[4] G. Rong, A. Mendez, E. B. Assi, B. Zhao, and M. Sawan, "Artificial intelligence in healthcare: review and prediction case studies," *Engineering*, vol. 6, no. 3, pp. 291–301, 2020.

[5] M. Senbekov, T. Saliev, Z. Bukeyeva, A. Almabayeva, M. Zhanaliyeva, N. Aitenova, Y. Toishibekov, I. Fakhradiyev, *et al.*, "The recent progress and applications of digital technologies in healthcare: a review," *International journal of telemedicine and applications*, vol. 2020, 2020.

[6] M. Veletic, E. H. Apu, M. Simic, J. Bergsland, I. Balasingham, C. H. Contag, and N. Ashammakhi, "Implants with sensing capabilities," *Chemical Reviews*, vol. 122, no. 21, pp. 16329–16363, 2022.

[7] M. L. Rocca, A. R. Palumbo, F. Visconti, and C. Di Carlo, "Safety and benefits of contraceptives implants: a systematic review," *Pharmaceuticals*, vol. 14, no. 6, p. 548, 2021.

[8] X. Huang, L. Wang, H. Wang, B. Zhang, X. Wang, R. Y. Stening, X. Sheng, and L. Yin, "Materials strategies and device architectures of emerging power supply devices for implantable bioelectronics," *Small*, vol. 16, no. 15, p. 1902827, 2020.

[9] Y. Lu, X. Wang, S. Mao, D. Wang, D. Sun, Y. Sun, A. Su, C. Zhao, X. Han, K. Li, *et al.*, "Smart batteries enabled by implanted flexible sensors," *Energy & Environmental Science*, vol. 16, no. 6, pp. 2448–2463, 2023.

[10] C. Y. Kim, M. J. Ku, R. Qazi, H. J. Nam, J. W. Park, K. S. Nam, S. Oh, I. Kang, J.-H. Jang, W. Y. Kim, *et al.*, "Soft subdermal implant capable of wireless battery charging and programmable controls for applications in optogenetics," *Nature communications*, vol. 12, no. 1, p. 535, 2021.

[11] H. Fu, X. Mei, D. Yurchenko, S. Zhou, S. Theodossiades, K. Nakano, and E. M. Yeatman, "Rotational energy harvesting for self-powered sensing," *Joule*, vol. 5, no. 5, pp. 1074–1118, 2021.

[12] F. Deng, X. Yue, X. Fan, S. Guan, Y. Xu, and J. Chen, "Multisource energy harvesting system for a wireless sensor network node in the field environment," *IEEE Internet of Things Journal*, vol. 6, no. 1, pp. 918–927, 2018.

[13] K. W. Choi, A. A. Aziz, D. Setiawan, N. M. Tran, L. Ginting, and D. I. Kim, "Distributed wireless power transfer system for internet of things devices," *IEEE Internet of Things Journal*, vol. 5, no. 4, pp. 2657–2671, 2018.

[14] J. S. Ho, A. J. Yeh, E. Neofytou, S. Kim, Y. Tanabe, B. Patlolla, R. E. Beygui, and A. S. Poon, "Wireless power transfer to deep-tissue microimplants," *Proceedings of the National Academy of Sciences*, vol. 111, no. 22, pp. 7974–7979, 2014.

[15] M. Song, P. Jayathurathnage, E. Zanganeh, M. Krasikova, P. Smirnov, P. Belov, P. Kapitanova, C. Simovski, S. Tretyakov, and A. Krasnok, "Wireless power transfer based on novel physical concepts," *Nature Electronics*, vol. 4, no. 10, pp. 707–716, 2021.

[16] K. W. Choi, S. I. Hwang, A. A. Aziz, H. H. Jang, J. S. Kim, D. S. Kang, and D. I. Kim, "Simultaneous wireless information and power transfer (swipt) for internet of things: Novel receiver design and experimental validation," *IEEE Internet of Things journal*, vol. 7, no. 4, pp. 2996–3012, 2020.

[17] H. Bhamra, J.-W. Tsai, Y.-W. Huang, Q. Yuan, J. V. Shah, and P. Irazoqui, "A subcubic millimeter wireless implantable intraocular pressure monitor microsystem," *IEEE Transactions on Biomedical Circuits and Systems*, vol. 11, no. 6, pp. 1204–1215, 2017.

[18] M. J. Karimi, A. Schmid, and C. Dehollain, "Wireless power and data transmission for implanted devices via inductive links: A systematic review," *IEEE Sensors Journal*, vol. 21, no. 6, pp. 7145–7161, 2021.

[19] H. Dinis, I. Colmiais, and P. Mendes, "Smart wireless-powering-enabling iot in inhomogeneous environments: A case study on biomedical applications," *IEEE Internet of Things Journal*, vol. 9, no. 22, pp. 23008–23016, 2022.

[20] O. Knecht and J. W. Kolar, "Performance evaluation of series-compensated ipt systems for transcutaneous energy transfer," *IEEE Transactions on Power Electronics*, vol. 34, no. 1, pp. 438–451, 2018.

[21] I. A. Shah and H. Yoo, "Assessing human exposure with medical implants to electromagnetic fields from a wireless power transmission system in an electric vehicle," *IEEE Transactions on Electromagnetic Compatibility*, vol. 62, no. 2, pp. 338–345, 2019.

[22] D. Kim, D. Jeong, J. Kim, H. Kim, J. Kim, S.-M. Park, and S. Ahn, "Design and implementation of a wireless charging-based cardiac monitoring system focused on temperature reduction and robust power transfer efficiency," *Energies*, vol. 13, no. 4, p. 1008, 2020.

[23] L. Qian, K. Qian, Y. Shi, H. Xia, J. Wang, and Y. Xia, "Tsv based orthogonal coils with high misalignment tolerance for inductive power transfer in biomedical implants," *IEEE Transactions on Circuits and Systems II: Express Briefs*, vol. 68, no. 6, pp. 1832–1836, 2020.

[24] Q. Wang, W. Che, M. Mongiardo, and G. Monti, "Wireless power transfer system with high misalignment tolerance for bio-medical implants," *IEEE Transactions on Circuits and Systems II: Express Briefs*, vol. 67, no. 12, pp. 3023–3027, 2020.

[25] X. Yi, W. Zheng, H. Cao, S. Wang, X. Feng, and Z. Yang, "Wireless power transmission for implantable medical devices using focused ultrasound and a miniaturized 1-3 piezoelectric composite receiving transducer," *IEEE Transactions on Ultrasonics, Ferroelectrics, and Frequency Control*, vol. 68, no. 12, pp. 3592–3598, 2021.

[26] S. Surappa and F. L. Degertekin, "Characterization of a parametric resonance based capacitive ultrasonic transducer in air for acoustic power transfer and sensing," *Sensors and Actuators A: Physical*, vol. 303, p. 111863, 2020.

[27] R. Hinchet, H.-J. Yoon, H. Ryu, M.-K. Kim, E.-K. Choi, D.-S. Kim, and S.-W. Kim, "Transcutaneous ultrasound energy harvesting using capacitive triboelectric technology," *Science*, vol. 365, no. 6452, pp. 491–494, 2019.

[28] A. Ibrahim, M. Meng, and M. Kiani, "A comprehensive comparative study on inductive and ultrasonic wireless power transmission to biomedical implants," *IEEE sensors journal*, vol. 18, no. 9, pp. 3813–3826, 2018.

[29] Y. Hong, L. Jin, B. Wang, J. Liao, B. He, T. Yang, Z. Long, P. Li, Z. Zhang, S. Liu, *et al.*, "A wood-templated unidirectional piezoceramic composite for transmuscular ultrasonic wireless power transfer," *Energy & Environmental Science*, vol. 14, no. 12, pp. 6574–6585, 2021.

[30] A. Javan-Khoshkholgh and A. Farajidavar, "Simultaneous wireless power and data transfer: Methods to design robust medical implants for gastrointestinal tract," *IEEE Journal of Electromagnetics, RF and Microwaves in Medicine and Biology*, vol. 6, no. 1, pp. 3–15, 2021.

[31] J. C. Chen, P. Kan, Z. Yu, F. Alrashdan, R. Garcia, A. Singer, C. E. Lai, B. Avants, S. Crosby, Z. Li, *et al.*, "A wireless millimetric magnetoelectric implant for the endovascular stimulation of peripheral nerves," *Nature Biomedical Engineering*, vol. 6, no. 6, pp. 706–716, 2022.

[32] M. Najjarzadegan, E. H. Hafshejani, and S. Mirabbasi, "An open-loop double-carrier simultaneous wireless power and data transfer system," *IEEE Transactions on Circuits and Systems II: Express Briefs*, vol. 66, no. 5, pp. 823–827, 2019.

[33] S. Sonmezoglu, J. R. Fineman, E. Maltepe, and M. M. Maharbiz, "Monitoring deep-tissue oxygenation with a millimeter-scale ultrasonic implant," *Nature Biotechnology*, vol. 39, no. 7, pp. 855–864, 2021.

[34] S. Gayen, B. Biswas, and A. Karmakar, "The quest for a miniaturized antenna in the wireless capsule endoscopy application: a review," *International Journal of Microwave and Wireless Technologies*, vol. 14, no. 9, pp. 1195–1205, 2022.

[35] H. Mirzajani, F. Mirlou, E. Istif, R. Singh, and L. Beker, "Powering smart contact lenses for continuous health monitoring: Recent advancements and future challenges," *Biosensors and Bioelectronics*, vol. 197, p. 113761, 2022.

[36] J. Lee, B. Bae, B. Kim, and B. Lee, "Full-duplex enabled wireless power transfer system via textile for miniaturized imd," *Biomedical Engineering Letters*, vol. 12, no. 3, pp. 295–302, 2022.

[37] C. Lee, B. Kim, J. Kim, S. Lee, T. Jeon, W. Choi, S. Yang, J.-H. Ahn, J. Bae, and Y. Chae, "A miniaturized wireless neural implant with body-coupled power delivery and data transmission," *IEEE Journal of Solid-State Circuits*, vol. 57, no. 11, pp. 3212–3227, 2022.

[38] I. A. Shah, A. Basir, Y. Cho, and H. Yoo, "Safety analysis of medical implants in the human head exposed to a wireless power transfer system," *IEEE Transactions on Electromagnetic Compatibility*, vol. 64, no. 3, pp. 640–649, 2022.

[39] M. L. Karim, A. M. Bosnjak, J. McLaughlin, P. Crawford, D. McEneaney, and O. J. Escalona, "Transcutaneous pulsed rf energy transfer mitigates tissue heating in high power demand implanted device applications: In vivo and in silico models results," *Sensors*, vol. 22, no. 20, p. 7775, 2022.

[40] Z. Kashani, S. J. Ilham, and M. Kiani, "Design and optimization of ultrasonic links with phased arrays for wireless power transmission to biomedical implants," *IEEE transactions on biomedical circuits and systems*, vol. 16, no. 1, pp. 64–78, 2022.

[41] A. Iqbal, P. R. Sura, M. Al-Hasan, I. B. Mabrouk, and T. A. Denidni, "Wireless power transfer system for deep-implanted biomedical devices," *Scientific Reports*, vol. 12, no. 1, p. 13689, 2022.

[42] G. Akoun and J.-P. Yonnet, "3d analytical calculation of the forces exerted between two cuboidal magnets," *IEEE Transactions on magnetics*, vol. 20, no. 5, pp. 1962–1964, 1984.

[43] H. Allag, J.-P. Yonnet, and M. E. Latreche, "3d analytical calculation of forces between linear halbach-type permanent-magnet arrays," in *2009 8th International Symposium on Advanced Electromechanical Motion Systems & Electric Drives Joint Symposium*. IEEE, 2009, pp. 1–6.

[44] H. Fu and E. M. Yeatman, "A methodology for low-speed broadband rotational energy harvesting using piezoelectric transduction and frequency up-conversion," *Energy*, vol. 125, pp. 152–161, 2017.

[45] A. Erturk and D. J. Inman, "An experimentally validated bimorph cantilever model for piezoelectric energy harvesting from base excitations," *Smart materials and structures*, vol. 18, no. 2, p. 025009, 2009.

[46] S.-H. Ahn, J. Jeong, and S. J. Kim, "Emerging encapsulation technologies for long-term reliability of microfabricated implantable devices," *Micromachines*, vol. 10, no. 8, p. 508, 2019.

[47] Y. Saito, H. Takao, T. Tani, T. Nonoyama, K. Takatori, T. Homma, T. Nagaya, and M. Nakamura, "Lead-free piezoceramics," *Nature*, vol. 432, no. 7013, pp. 84–87, 2004.

[48] A. Ameye, N. Decroix, D. Gibus, N. Garraud, P. Gasnier, and A. Badel, "Increasing the robustness of electrodynamic wpt systems with hybrid electromechanical transduction," *Smart Materials and Structures*, vol. 33, no. 2, p. 025002, 2024.

[49] B. D. Truong, E. Andersen, C. Casados, and S. Roundy, "Magnetoelectric wireless power transfer for biomedical implants: Effects of non-uniform magnetic field, alignment and orientation," *Sensors and Actuators A: Physical*, vol. 316, p. 112269, 2020.

[50] V. S. Crasto, M. G. Stormant, and D. P. Arnold, "A three-phase rotating magnet electrodynamic wireless power transmission receiver," in *2023 IEEE SENSORS*. IEEE, 2023, pp. 1–4.

[51] M. A. Halim, A. A. Rendon-Hernandez, S. E. Smith, and D. P. Arnold, "A chip-sized piezoelectric receiver for low-frequency, near-field wireless power transfer: Design, modeling and experimental validation," *Smart Materials and Structures*, vol. 30, no. 4, p. 045011, 2021.

[52] S. E. Smith, M. A. Halim, A. A. Rendon-Hernandez, and D. P. Arnold, "Dual-transduction electromechanical receiver for near-field wireless power transmission," in *2021 IEEE 34th International Conference on Micro Electro Mechanical Systems (MEMS)*. IEEE, 2021, pp. 38–41.

[53] Y. Wu, H. Yuan, R. Zhang, A. Yang, X. Wang, and M. Rong, "Low-frequency wireless power transfer via rotating permanent magnets," *IEEE Transactions on Industrial Electronics*, vol. 69, no. 10, pp. 10 656–10 665, 2022.

[54] Q. Cao, R. Deng, Y. Pan, R. Liu, Y. Chen, G. Gong, J. Zou, H. Yang, and D. Han, "Robotic wireless capsule endoscopy: recent advances and upcoming technologies," *Nature Communications*, vol. 15, no. 1, p. 4597, 2024.

[55] M. Haerinia and R. Shadid, "Wireless power transfer approaches for medical implants: A review," *Signals*, vol. 1, no. 2, pp. 209–229, 2020.